ChemComm

COMMUNICATION

Cite this: *Chem. Commun.*, 2016, **52**, 8455

Received 28th April 2016,
Accepted 13th June 2016

DOI: 10.1039/c6cc03579e

www.rsc.org/chemcomm

Reversible photo-patterning of soft conductive materials *via* spatially-defined supramolecular assembly†

Xun He, Jingwei Fan, Jiong Zou and Karen L. Wooley*

A strategy for reversible patterning of soft conductive materials is described, based upon a combination of peptide-based block copolymer hydrogelators and photo-thermally-active carbon nanotubes. This composite displays photo-responsive gelation at application-relevant timescales (<10 s), allowing for rapid and spatially-defined construction of conductive patterns (>100 S m^{-1}), which, additionally, hold the capability to revert to sol upon sonication for reprocessing.

The recent five years have witnessed the development of reversible photo-printing technologies, which include pioneering work to apply reversible covalent bond exchange reactions on functionalized surfaces, for light-healable coatings, repairable microarray technologies and patterned synthetic biomaterials, among others.[1–3] Nevertheless, the requirement on initial surface functionalization may complicate the process and limit the choice of available substrates. Being able to circumvent this complication, supramolecular assembly *via* noncovalent interactions has been applied in patterning through photo-triggered molecular assembly and subsequent sol–gel transitions, as the assembly process can occur without reliance on reactive functional groups on substrates.[4–6] In addition, supramolecular assembly usually possesses reversibility and stimuli-responsiveness, and, therefore, is a competitive approach to develop smart and reprocessable materials.[7]

Inspired by the reversible printing techniques and advantages of supramolecular assembly outlined above, we designed a new strategy that integrates conductive materials into stimuli-responsive gelators for rapid and reversible construction of conductive soft materials with spatiotemporal definition *via* supramolecular assembly. This strategy was created as an approach to the current challenge to print reprocessable and rewritable conductive materials, as previous photo-patterning process typically relies on irreversible, and thus 'dead' reactions.[8,9] In this design, it was expected that a cascading series of events would occur, by which a photo-thermal conductive material would absorb light and generate heat, to be absorbed by a thermo-responsive hydrogelator, resulting in a triggered supramolecular assembly process and affording conductive, patterned, flexible materials. Based upon the demonstration of this strategy reported herein, a broad scope of applications can be anticipated, including patternable and flexible conductive materials with various dimensions, injectable and near IR curable hydrogels for bioelectronics or tissue engineering, and 3D printing materials for permanent or temporary layers.

The thermo-responsive hydrogelator employed in this study was comprised of the amphiphilic block copolymer poly(ethylene glycol)-*block*-poly(DL-allylglycine) (PEG-*b*-PDLAG). This and similar β-sheet-rich polypeptides have displayed reversible gelation in response to heat and sonication.[10] Synthesis of a series of three PEG-*b*-PDLAGs was performed through polymerization of the *N*-carboxyanhydride (NCA) of DL-allylglycine *via* a N_2 flow method (Fig. S1, ESI†), to tune the hydrophilic–hydrophobic balance and optimize the gel transition temperature (T_{gel}) to be slightly above room temperature.[11] Reversible and responsive hydrogelations of PEG-*b*-PDLAG were confirmed (Fig. S3, ESI†). The heat-induced sol-to-gel transitions were attributed to the constrution of β sheets and dehydration of PEG, resulting in the formation of β-sheet-rich peptide nanofibrils (Scheme 1a); while the sonication-triggered gel-to-sol transitions were assigned to the disruption of long range interactions between these nanofibrils.[12,13] In this way, the sol–gel transitions were correlated with reversible noncovalent transformation of supramolecularly-assembled nanostructures instead of chemical bond conversion, thus, no additional chemicals, such as a photoacid generator or exchange reagent, were needed.

For the conductive component, single-walled carbon nanotubes (SWCNTs) were selected, due to their excellent electrical conductivity, mechanical strength, high aspect ratio, and photo-thermal effect.[14–20] In order to be solution-processable, SWCNTs have been dispersed through interaction with a wide

Departments of Chemistry, Chemical Engineering, and Materials Science & Engineering, Laboratory for Synthetic-Biologic Interactions, Texas A&M University, 3255 TAMU, College Station, TX 77842, USA. E-mail: wooley@chem.tamu.edu

† Electronic supplementary information (ESI) available: Materials, characterization techniques, synthetic details, NMR spectra, sol–gel phase diagrams, photographs, UV/vis spectra, Raman spectrum, conductivity data, *I–V* curves, film parameter table. See DOI: 10.1039/c6cc03579e

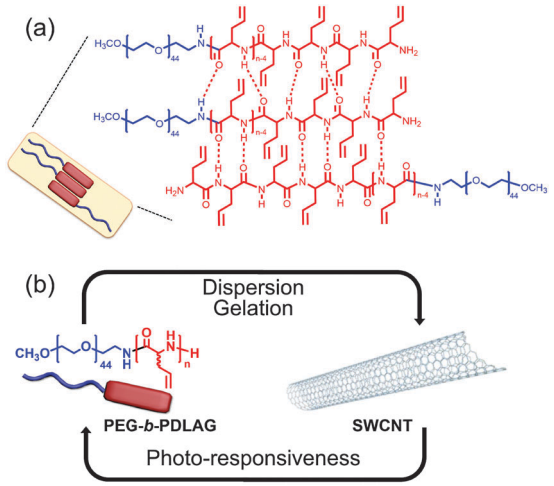

Scheme 1 (a) Illustrative formation of β sheets as constructive units of nanofibrils. (b) Relationships between the functions of the PEG-*b*-PDLAG and SWCNT composite components.

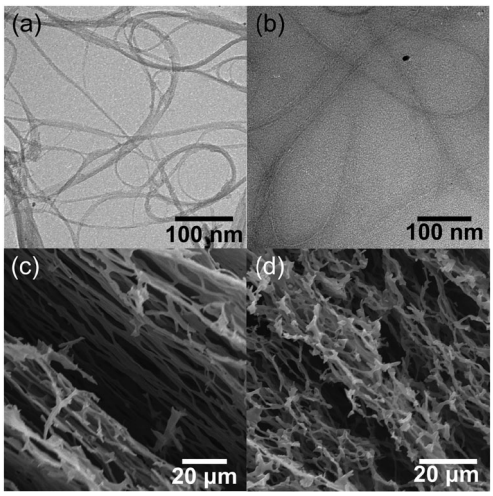

Fig. 1 TEM images of (a) SWCNT sol and (b) PEG-*b*-PDLAG/SWCNT composite sol, without staining. SEM images of aerogels of (c) 5 wt% PEG-*b*-PDLAG and (d) 5 wt% PEG-*b*-PDLAG/0.5 wt% SWCNT composite.

variety of conjugated structures.[21,22] One of the conjugated structures reported was allyl-rich β-sheet peptide domain, which has been shown to interact with SWCNT surfaces for dispersion, and display hierarchically-ordered assembly behaviors.[23] Therefore, it was anticipated that the π–π stacking between the pseudo-aligned allyl groups of PDLAGs and SWCNT surfaces could allow for dispersion of the nanotubes in water, facilitated by the amphiphilic polymers. The working hypothesis for the overall cascading strategy was that there would be a stagewise synergistic effect that would translate the photo-thermal behavior of SWCNTs to a thermo-induced gelation of the polymers, to result in photo-triggered spatially-defined gelation and patterning (Scheme 1b).

Preparation of the composite sol dispersion was industry-friendly as it merely required 10 min sonication after direct mixing of the two components in nanopure water, as confirmed visually (Fig. S4, ESI†) and by UV/vis spectroscopy (Fig. S5, ESI†).[24] Herein, PEG-*b*-PDLAG served as both a dispersant and a stimuli-responsive component. Dispersion was further characterized microscopically by comparing the difference in transmission electron microscopic (TEM) images between freshly sonicated SWCNT and PEG-*b*-PDLAG/SWCNT composite sol (Fig. 1a and b), as the composite exhibited better dispersion and less aggregation into bundles.

PEG-*b*-PDLAG/SWCNT hydrogels were prepared by heating sols to their T_{gel} values, which decreased upon the addition of SWCNTs (Fig. S6, ESI†). Scanning electron microscopic (SEM) images showed fibrillar network structures, but with different fibrillar curvature, for matrices of PEG-*b*-PDLAG with and without SWCNTs, indicating SWCNTs affected or participated in the formation of composite gel matrix (Fig. 1c and d). As expected, composite gels at 1 wt% SWCNT expressed higher stiffness in dynamic mechanical analysis (DMA), compared with polymer gels (Fig. 2a), which can be attributed to the high mechanical strength and a certain extent of entanglement of SWCNTs in the composite. However, the depressed stiffness

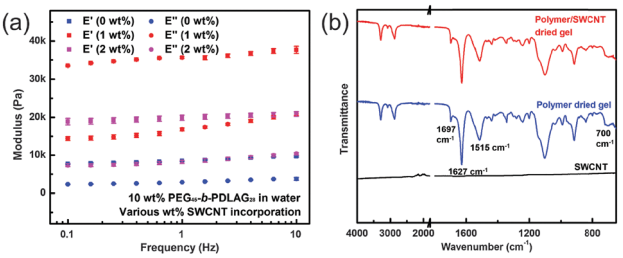

Fig. 2 (a) Moduli of PEG-*b*-PDLAG/SWCNT hydrogels as a function of frequency conducted by DMA (*E′* and *E″* indicate storage and loss modulus, respectively). (b) IR spectra of polymer/SWCNT aerogel, polymer aerogel, and SWCNTs.

with even higher (2 wt%) SWCNT incorporation might be a result of the over-consumption of the gelators in dispersing the nanotube fillers, resulting in a difficulty to form an interconnected network. In order to understand the potential driving force for gelation, IR spectroscopy was utilized to examine the supramolecular structure within freeze-dried samples. The IR spectra of polymer and polymer/SWCNT composite were almost identical, with the presence of signatures of β-sheet secondary structures, demonstrating that formation of β-sheet structures remained as a potential driving force for the gelation of the composite (Fig. 2b).[25]

Based on the dispersion and gelation studies, the stimuli-responsive behaviors were then explored to verify the feasibility of our material design. In addition to thermo- and sonication-responsive behaviors, it is worth noting that irradiation of the composite sol with light (532 nm or 785 nm, 250 mW, 2 mm diameter laser beam) induced sol-to-gel transitions (Fig. 3a), agreeing with our hypothesis on the synergistic photo-to-thermal cascading effects. Moreover, either the sols or gels were highly sensitive towards light, heat or mechanical stimulus, as controllable sol–gel transitions typically took place within 10 seconds. The differences of nanostructural morphologies were then visualized

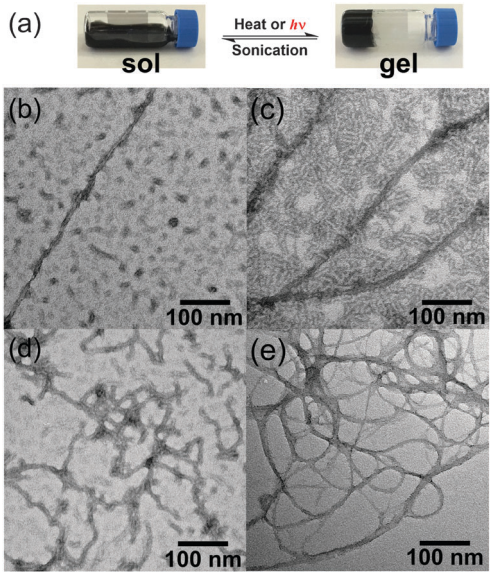

Fig. 3 (a) Reversible stimuli-responsive sol–gel transitions of the composite material having 5 wt% PEG-*b*-PDLAG and 0.5 wt% SWCNT. TEM images of (b) PEG-*b*-PDLAG/SWCNT composite sol, (c) PEG-*b*-PDLAG/SWCNT composite gel, (d) PEG-*b*-PDLAG gel, and (e) SWCNT sol, with phosphotungstic acid stain. For each TEM image, the sample concentrations were at 1 mg mL^{-1} PEG-*b*-PDLAG and 0.1 mg mL^{-1} SWCNT, if applicable.

by TEM to further study the dispersion and phase transition mechanisms. In TEM images, polymers adopted shapes as spherical aggregates and short nanofibrils in sol (Fig. 3b), and converted reversibly to longer nanofibrils with inter-fibrillar interactions and entanglements in the gel state (Fig. 3c). These transformations of polymeric nanostructures accounted for the sol–gel transitions on a macroscale (Scheme 2). On the other hand, SWCNTs in both sol and gel states (Fig. 3b and c) remained as longer fibers with less curvature, compared with polymer nanofibrils in the absence of SWCNT (Fig. 3d). Furthermore, the stained composite nanotubes displayed larger diameters (Fig. 3b: 15.3 ± 4.0 nm, and Fig. 3c: 18.9 ± 3.6 nm), compared with unstained composite nanotubes (Fig. 1b, 2.4 ± 0.4 nm). Due to staining of the polymers in the sample, the width increase can then be attributed to the non-covalent attachment of polymers on nanotube surfaces, and, thus, resulting in nanotube dispersion (*vide supra*).

The potential application of this smart composite system as patternable and rewritable conductive materials was then

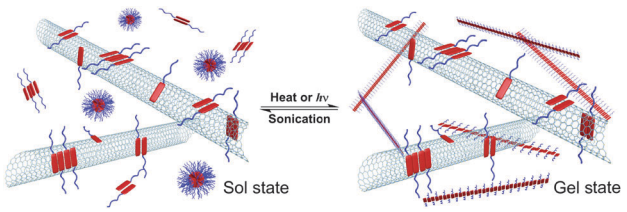

Scheme 2 Schematic illustration of a PEG-*b*-PDLAG/SWCNT dispersion, and reversible conversion of polymeric supramolecular structures that correlates to the formation or break-down of gel matrix in response to a stimulus.

investigated, taking advantage of the rapid and reversible phase transition through supramolecular assembly. As an example for the patterning process, the composite sol was applied to a glass substrate, then followed by direct irradiation with a laser beam. The irradiated region underwent a photo-curing process, giving a sol-to-gel transition and producing a spatially-defined gel pattern that remained on the surface after removal of the sol (Fig. 4a). The gel could be reverted to sol by sonication, or could be air dried to produce a composite film, which can be recycled as well for another writing process. Electrical conductivities of dried composite films were determined by four point probe measurements. For a composite film with 25 wt% SWCNT (derived from a pre-gelled film of a 7.5 wt% PEG_{45}-*b*-$PDLAG_{28}$/2.5 wt% SWCNT sample, followed by allowing the film to dry under ambient conditions and heat-pressing), the electrical conductivity was determined to be *ca.* 130 S m^{-1} (Fig. 4b), which is comparable to the highest reported values of hybrid films derived from conductive hydrogels that typically contain conductive polymers.[26] To further examine the reversibility and recyclability, electrical conductivities of composite films of up to three reprocessing cycles were obtained and found to remain similar after repeated recycling (Fig. S8, ESI†). Moreover, a printed free standing thin film was fabricated into a Möbius strip (Fig. 4c), suggesting that these thin films are flexible towards bending and twisting for soft electronics.

In summary, we developed a hydrogel-based block copolymeric/inorganic composite system that exhibited a wide range of thermo-, mechano- and photo-responsive properties. These materials are highly processable with assorted stimuli inputs, including temperature increase or photo irradiation for gelation and patterning, and sonication for material recycling. Furthermore, this system provided a novel method to process conductive materials in a liquid phase, followed by facile and rapid curing into desired patterns with the potential to take advantage of the modern

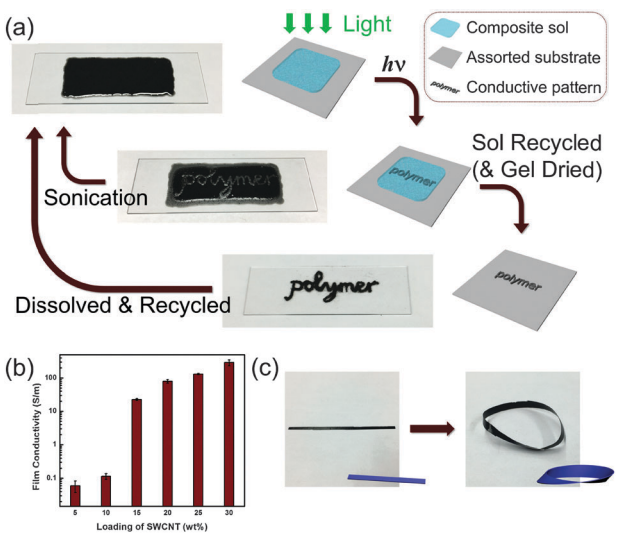

Fig. 4 (a) Schematic illustration of the reversible photo-patterning process for production of soft electronics. (b) Electrical conductivity of composite films (PEG_{45}-*b*-$PDLAG_{28}$/SWCNT) as a function of percentage SWCNT incorporation. (c) A printed free standing thin film fabricated into a Möbius strip.

photo stereolithographic technologies, without the requirement of a pre-treated substrate or a specific irradiation wavelength. The application of this composite system into 3D conductive networks for energy storage devices and neural signal harvesting are subjects of our current investigations.

This research was supported by the National Science Foundation (DMR-1105304, DMR-1507429, and DMR-1309724), the National Institutes of Health (HHSN268201000046C), and the Welch Foundation (W. T. Doherty-Welch Chair, A-0001). We thank Dariya Reid and Jodie L. Lutkenhaus in Chemical Engineering, and Peng Li and Hung-Jue Sue in Mechanical Engineering at Texas A&M University for providing instrumentation to perform hot-press and conductivity measurements, respectively. TEM and SEM imaging was conducted using instrumentation available in the Microscopy Imaging Center (MIC) at Texas A&M University.

References

1 X. Du, J. Li, A. Welle, L. Li, W. Feng and P. A. Levkin, *Adv. Mater.*, 2015, **27**, 4997–5001.
2 N. R. Gandavarapu, M. A. Azagarsamy and K. S. Anseth, *Adv. Mater.*, 2014, **26**, 2521–2526.
3 S. Arumugam and V. V. Popik, *J. Am. Chem. Soc.*, 2012, **134**, 8408–8411.
4 E. R. Draper, E. G. B. Eden, T. O. McDonald and D. J. Adams, *Nat. Chem.*, 2015, **7**, 848–852.
5 C. Maity, W. E. Hendriksen, J. H. van Esch and R. Eelkema, *Angew. Chem., Int. Ed.*, 2015, **54**, 998–1001.
6 D. J. Cornwell, O. J. Daubney and D. K. Smith, *J. Am. Chem. Soc.*, 2015, **137**, 15486–15492.
7 X. Yan, F. Wang, B. Zheng and F. Huang, *Chem. Soc. Rev.*, 2012, **41**, 6042–6065.
8 J. Du, S. Pei, L. Ma and H.-M. Cheng, *Adv. Mater.*, 2014, **26**, 1958–1991.
9 G. Sun, S. Cho, C. Clark, S. V. Verkhoturov, M. J. Eller, A. Li, A. Pavía-Jiménez, E. A. Schweikert, J. W. Thackeray, P. Trefonas and K. L. Wooley, *J. Am. Chem. Soc.*, 2013, **135**, 4203–4206.
10 X. He, J. Fan and K. L. Wooley, *Chem. – Asian J.*, 2016, **11**, 437–447.
11 J. Zou, J. Fan, X. He, S. Zhang, H. Wang and K. L. Wooley, *Macromolecules*, 2013, **46**, 4223–4226.
12 X. He, J. Fan, F. Zhang, R. Li, K. A. Pollack, J. E. Raymond, J. Zou and K. L. Wooley, *J. Mater. Chem. B*, 2014, **2**, 8123–8130.
13 J. Fan, J. Zou, X. He, F. Zhang, S. Zhang, J. E. Raymond and K. L. Wooley, *Chem. Sci.*, 2014, **5**, 141–150.
14 J. Wen, Y. Xu, H. Li, A. Lu and S. Sun, *Chem. Commun.*, 2015, **51**, 11346–11358.
15 S. Huang, C. Zhao, W. Pan, Y. Cui and H. Wu, *Nano Lett.*, 2015, **15**, 1609–1614.
16 S. N. Habisreutinger, T. Leijtens, G. E. Eperon, S. D. Stranks, R. J. Nicholas and H. J. Snaith, *Nano Lett.*, 2014, **14**, 5561–5568.
17 X. Zhang, Z. Yu, C. Wang, D. Zarrouk, J.-W. T. Seo, J. C. Cheng, A. D. Buchan, K. Takei, Y. Zhao, J. W. Ager, J. Zhang, M. Hettick, M. C. Hersam, A. P. Pisano, R. S. Fearing and A. Javey, *Nat. Commun.*, 2014, **5**, 2983.
18 C. Liang, S. Diao, C. Wang, H. Gong, T. Liu, G. Hong, X. Shi, H. Dai and Z. Liu, *Adv. Mater.*, 2014, **26**, 5646–5652.
19 P.-Y. Chen, M. N. Hyder, D. Mackanic, N.-M. D. Courchesne, J. Qi, M. T. Klug, A. M. Belcher and P. T. Hammond, *Adv. Mater.*, 2014, **26**, 5101–5107.
20 M. T. Byrne and Y. K. Gun'ko, *Adv. Mater.*, 2010, **22**, 1672–1688.
21 D. Tasis, N. Tagmatarchis, A. Bianco and M. Prato, *Chem. Rev.*, 2006, **106**, 1105–1136.
22 S. K. Samanta, M. Fritsch, U. Scherf, W. Gomulya, S. Z. Bisri and M. A. Loi, *Acc. Chem. Res.*, 2014, **47**, 2446–2456.
23 J. Zou, X. He, J. Fan, J. E. Raymond and K. L. Wooley, *Chem. – Eur. J.*, 2014, **20**, 8842–8847.
24 R. Haggenmueller, S. S. Rahatekar, J. A. Fagan, J. Chun, M. L. Becker, R. R. Naik, T. Krauss, L. Carlson, J. F. Kadla, P. C. Trulove, D. F. Fox, H. C. DeLong, Z. Fang, S. O. Kelley and J. W. Gilman, *Langmuir*, 2008, **24**, 5070–5078.
25 J. Zou, F. Zhang, Y. Chen, J. E. Raymond, S. Zhang, J. Fan, J. Zhu, A. Li, K. Seetho, X. He, D. J. Pochan and K. L. Wooley, *Soft Matter*, 2013, **9**, 5951–5958.
26 Y. Shi, M. Wang, C. Ma, Y. Wang, X. Li and G. Yu, *Nano Lett.*, 2015, **15**, 6276–6281.

